# Theory of optical properties of II-VI semiconductor quantum dots containing a single magnetic ion in a strong magnetic field

Anna H. Trojnar,[1,2] Marek Korkusiński,[1] Marek Potemski,[3] and Pawel Hawrylak[1,2]
[1]*Quantum Theory Group, Institute for Microstructural Sciences, National Research Council, Ottawa, Canada K1A0R6*
[2]*Department of Physics, University of Ottawa, Ottawa, Canada*
[3]*Grenoble High Magnetic Field Laboratory, CNRS Grenoble, France*
(Received 3 November 2011; published 6 April 2012)

We present a microscopic theory of the magnetic field dependence of the optical properties of II–VI semiconductor quantum dots containing a single magnetic (Mn) impurity. The single-particle electron and heavy-hole states are described exactly by two-dimensional harmonic oscillators in a magnetic field, the Mn ion is treated as a spin of an isoelectronic impurity, and the quantum dot anisotropy is included perturbatively. The electron-hole direct, short-, and long-range exchange electron-hole Coulomb interactions, as well as the short-range spin-spin contact exchange interaction of the electron and the hole with the magnetic impurity is included. The electron-hole-Mn states are expanded in a finite number of configurations controlled by the number of confined electronic quantum dot shells and the full interacting Hamiltonian is diagonalized numerically in this basis. The absorption and emission spectrum is predicted as a function of photon energy, magnetic field, number of confined shells, and anisotropy. It is shown that the magnetic-field-induced enhancement of the exchange interaction of the Mn spin with the exciton is largely canceled by increased electron-hole Coulomb interactions. The predicted weak magnetic field dependence of the spacing of emission lines agrees well with the results of the spin model at low magnetic fields but differs at higher magnetic fields. Correlations in the exciton-Mn complex are predicted to determine absorption spectra.

DOI: 10.1103/PhysRevB.85.165415 PACS number(s): 78.67.Hc, 71.70.Gm, 78.55.Et, 73.21.La

## I. INTRODUCTION

There is currently interest in developing control over single spins in solid-state systems,[1–10] including the spin of a single manganese (Mn) ion in CdTe[11,12] semiconductor quantum dots.[10,13–17] The Mn ion with the magnetic moment $M = 5/2$ has been detected by observation of a characteristic excitonic emission spectrum consisting of six emission lines related to the $2M + 1 = 6$ quantum states of Mn.[10,16,18,19] The excitonic emission spectrum has been explained on the basis of a spin model where the exciton fine structure is represented by a single electron and valence hole spin interacting with the spin of the Mn ion.[10,15–20] In the spin model there are no correlations between the electron and the hole, and the electron spin-Mn spin and hole spin-Mn spin exchange are treated as constants. By applying a strong magnetic field we modify the electron and hole energy levels and wave functions. By increasingly localizing the electron and hole wave function in the quantum dot, one expects to increase the strength of electron(hole)-Mn exchange interaction and hence significantly modify the optical properties of semimagnetic quantum dots. However, recent experiments[10,19,20] indicate that the emission properties do not change significantly with the magnetic field and can be described by a magnetic-field-independent spin model.

To address this puzzle we develop here a microscopic theory of correlated electron-hole complexes which allows one to calculate the emission and absorption spectrum of quantum dots containing a single magnetic ion in a strong magnetic field. We demonstrate that while the magnetic field enhances the interaction of exciton ($X$) with the Mn ion leading to a magnetic field-induced increase in the spacing of emission peaks, the magnetic field-induced increase of Coulomb interactions and correlations in the $X$-Mn system cancel the increase in the $X$-Mn coupling. This cancellation makes the spin model superficially agree with the experiment.

Theory of electronic correlations in quantum dots with Mn ions has been developed already, including transport,[13,21,22] tuning of the QD magnetization by changing the number of carriers,[23–28] and theory of far-infrared spectroscopy.[29,30] The theory of optical properties and coherent control was also developed but without the simultaneous inclusion of electron and hole shell structure, electron-hole correlations, quantum dot anisotropy, electron-hole exchange, and magnetic field.[18,31–33]

In our previous work[34] a fully microscopic model of exciton[35,36] coupled to the Mn ion has been developed. A quantum interference (QI) effect between the electron-hole Coulomb scattering and the scattering by the Mn ion was predicted to significantly affect the exciton-Mn coupling and emission and absorption spectra. In parallel, a theory of exciton fine structure in an arbitrary magnetic field[37] extended the theory of an exciton in a magnetic field presented in Refs. 38–40.

Here we extend the microscopic model of the exciton-Mn system presented previously by us in Ref. 34 to high magnetic fields. Using exact diagonalization techniques for the exciton-Mn Hamiltonian we predict the evolution of the absorption and emission spectra with the magnetic field for quantum dots with different shell structure, anisotropy, and Mn-ion position. This allows one to predict the signature of the Mn ion in the absorption spectra of excited quantum dot shells as well as to compare the emission spectrum from a correlated $X$-Mn complex with the simplified spin model.

The paper is organized as follows. Section II describes the model of the quantum dot and its single-particle states. Section III describes an exciton confined in a QD and its

interaction with the Mn impurity. Section IV derives the spin model Hamiltonian, while Sec. V explains emission and absorption calculations. Results and their discussion are presented in Sec. VI. A summary is contained in Sec. VII.

## II. THE MODEL AND THE SINGLE-PARTICLE SPECTRUM

We study a quasi-two-dimensional anisotropic parabolic quantum dot in a perpendicular magnetic field[41,42] in the effective-mass approximation (EMA). We divide the confining potential into the isotropic, parabolic part and the anisotropic correction. The isotropic two-dimensional parabolic potential was shown to be a good approximation for the self-assembled QDs,[38–40] while the effects of the anisotropy are visible in the exciton fine structure[43] and the splitting of the $p$ shell.[44] The strain in QDs splits the light- and heavy-hole states at the top of the valence band.[45] This allows us to neglect the light holes and consider the heavy holes only with spin projection on the growth axis $\tau_{hh} = \pm 3/2$.

In what follows, the energy is measured in effective Rydbergs ($\mathcal{R}^* = m^* e^4/2\varepsilon^2\hbar^2$), and distances in Bohr radius ($a_B = \varepsilon\hbar^2/m_e^* e^2$), where $m_e^*$ is the effective mass of the electron, $e$ is the electron charge, $\varepsilon$ is the dielectric constant of the material, and $\hbar$ is the reduced Planck constant.

We define our basis in terms of eigenstates of the isotropic parabolic quantum dot. The envelope functions $|i\sigma\rangle(|j\tau\rangle)$ are single-particle states of the electron (hole) in an isotropic parabolic confining potential with characteristic frequency $\Omega_0^{e(h)}$ in the presence of a magnetic field perpendicular to the plane of the quantum dot.[40–42] Index $i(j)$ denotes here the set of harmonic oscillator (HO) numbers $i = \{n_+, n_-\}$. It corresponds to the eigenenergy $\varepsilon_{n_+ n_- \sigma}^{e(h)} = \Omega_+^{e(h)}(n_+ + \frac{1}{2}) + \Omega_-^{e(h)}(n_- + \frac{1}{2}) + g_{e(h)}\mu_B B\sigma$,[38,41] where $\Omega_\pm^{e(h)} = \Omega_h^{e(h)} \pm \frac{1}{2}\Omega_c^{e(h)}$ and the hybrid frequency $\Omega_h^{e(h)} = \sqrt{\Omega_0^{e(h)2} + \frac{1}{4}\Omega_c^{e(h)2}}$ and cyclotron energy $\Omega_c^{e(h)} = eB/m_{e(h)}^* c$ (with $c$ being the speed of light) are expressed in Rydbergs.

## III. THE CORRELATED EXCITON-Mn MODEL

### A. Exciton

The correlated exciton-Mn system without the magnetic field was described by us in Ref. 34. The exciton in a magnetic field, including the electron-hole exchange and anisotropy was discussed in Ref. 37. For completeness we summarize here the basic theoretical steps. We start with the electron-hole Hamiltonian in the isotropic parabolic quantum dot with single-particle HO states $i$, energies $\varepsilon_{i,\tau}^{e(h)}$, and only direct Coulomb interaction matrix elements[46,47] $\langle i,j|V|k,l\rangle$ in the form

$$\hat{H}_{EH} = \sum_{i,\tau} \varepsilon_{i,\tau}^h h_{i,\tau}^+ h_{i,\tau} + \sum_{i,\sigma} \varepsilon_{i,\sigma}^e c_{i,\sigma}^+ c_{i,\sigma} - \sum_{ijkl,\sigma\tau} \langle i,j|V|k,l\rangle c_{i\sigma}^+ h_{j\tau}^+ h_{k\tau} c_{l\sigma}, \quad (1)$$

where $h_{i\tau}^+$ ($c_{i\sigma}^+$) and $h_{i\tau}$ ($c_{i\sigma}$) create and annihilate the hole (electron) on the orbital $i$ with the spin $\tau(\sigma)$.

The Hamiltonian of an exciton in a QD with an isotropic confining potential commutes with both the exciton angular momentum $L = n_+^e - n_-^e + n_-^h - n_+^h$ and spin operators. We construct electron-hole configurations for each total angular momentum $L$ in the form $|L;ij\rangle = h_i^+ c_j^+|\text{vac}\rangle$.

In each $L$ subspace and for each value of the magnetic field $B$ the Hamiltonian matrices (1) are built and diagonalized numerically. This gives a set of eigenstates in the form of linear combinations of basis configurations: $|X_k^L\rangle = \sum_{(ij)}^{N_L} A_{L;ij}^{(k)}|L;ij\rangle$ with energy $E_k^L$, where $k = 1,\ldots,N_L$, and $N_L$ is the size of the basis with angular momentum $L$, and $A_{L;ij}^{(k)}$ is the amplitude of configuration $|L;ij\rangle$ in state $|X_k^L\rangle$. Each of these states is fourfold degenerate due to the four possible electron and hole spin alignments. The coefficients $A_{L;ij}^{(k)}$ as well as the exciton energies depend on the magnetic field $B$, and are evaluated for each $B$ separately. All angular momenta and spin states are needed because the electron-hole exchange as well as the exciton interaction with the Mn ion mixes $X$ states with different angular momenta and spins.

### B. Electron-hole exchange, anisotropy, and coupling of exciton with Mn ion

We now include the electron-hole exchange,[43,48–52] the quantum dot anisotropy, and the exchange interaction of electron (hole) with the Mn ion. The interacting electron-hole-Mn system is described by the Hamiltonian[32]

$$H_X = H_{EH} + H_{EHX} + H_{\text{anis}} + H_{\text{Zeeman}} + H_{h\text{-Mn}} + H_{e\text{-Mn}}. \quad (2)$$

The first term is the electron-hole Hamiltonian $H_{EH}$ (1) discussed above. The second term is the electron-hole exchange term in the magnetic field[37]

$$H_{EHX} = \sum_{ijkl\sigma\sigma'\tau\tau'} \langle i\sigma, j\tau|V_{eh}^X|k\tau', l\sigma'\rangle c_{i\sigma}^+ h_{j\tau}^+ h_{k\tau'} c_{l\sigma'}.$$

The third is the anisotropic potential term $H_{\text{anis}} = \sum_{ij\tau} t_{ij}^h h_{i\tau}^+ h_{j\tau} + \sum_{ij\sigma} t_{ij}^e c_{i\sigma}^+ c_{i\sigma}$, which breaks the cylindrical symmetry of the quantum dot and mixes the single-particle states with different angular momenta. In Ref. 37 we have presented details of our treatment of the electron-hole exchange and anisotropy in the magnetic field. Here let us only state that the effect of anisotropy is included by allowing for the parabolic potentials in the $x,y$ directions to be different. The characteristic frequency of the cylindrically symmetric component of the parabolic confinement can now be expressed in terms of two confinement frequencies as $\Omega_{0,e(h)}^2 = \frac{1}{2}(\Omega_{x,e(h)}^2 + \Omega_{y,e(h)}^2)$, while the anisotropic component $t_{ij}^{e(h)}$ is proportional to the anisotropy parameter $\gamma_{e(h)} = (\Omega_{x,e(h)}^2 - \Omega_{y,e(h)}^2)/(\Omega_{x,e(h)}^2 + \Omega_{y,e(h)}^2)$.

The fourth term is the Zeeman energy of the magnetic ion, the hole, and the electron $H_{\text{Zeeman}} = g_{Mn}\mu_B B M_Z + g_e\mu_B B S_Z + g_h\mu_B B j_Z$, where $g_{\text{Mn}}$, $g_e$, and $g_h$ are the Mn ion, electron, and hole Landé $g$ factors, respectively, and $\mu_B$ is the Bohr magneton. $M_Z$, $S_Z$, and $j_Z$ are the Mn-, electron-, and heavy-hole-spin $z$ projections, respectively.

The hole-Mn Hamiltonian

$$H_{h\text{-Mn}} = \sum_{i,j} \frac{3J^h_{ij}(R)}{2}[(h^+_{i,\Uparrow}h_{j,\Uparrow} - h^+_{i,\Downarrow}h_{j,\Downarrow})M_Z] \qquad (3)$$

describes the scattering of the hole by the Mn ion at position $R$, while conserving the hole spin. $J^h_{ij}(R)$ is the hole-Mn exchange matrix element leading to the scattering of a hole from state $i$ to state $j$ by the Mn ion at position $R$,[23,32] defined as $J^h_{ij}(R) = J^h_{2D}\Psi^*_i(R)\Psi_j(R)$, where $J^h_{2D} = 2J^h_{(0)}/d$, with $J^h_{(0)}$ being the bulk hole-Mn coupling constant and $d$ the height of the QD. This scattering process does depend on the state $M_Z$ of the Mn spin as well as on $R$. The electron-Mn interaction term is similar to the hole-Mn scattering term except for the sign and the additional spin-flipping term

$$H_{e\text{-Mn}} = -\sum_{i,j} \frac{J^e_{ij}(R)}{2}[(c^+_{i,\uparrow}c_{j,\uparrow} - c^+_{i,\downarrow}c_{j,\downarrow})M_Z + c^+_{i,\downarrow}c_{j,\uparrow}M^+ + c^+_{i,\uparrow}c_{j,\downarrow}M^-]. \qquad (4)$$

### C. Exciton-Mn basis

Having calculated the excitonic states $|X^L_k\rangle$, one generates the $X$-Mn basis states by multiplying each excitonic state by the electron-hole spin-wave function $|\sigma,\tau\rangle$ and by the Mn spin-wave function $|M_Z\rangle$ with $M_Z = \pm 5/2, \pm 3/2, \pm 1/2$. Thus, the $X$-Mn basis configurations are of the form $|X^L_k,\tau\sigma,M_Z\rangle = |X^L_k\rangle \otimes |\tau\sigma\rangle \otimes |M_Z\rangle$.

The nonzero elements of the $e$-Mn Hamiltonian (4) consist of two parts: one is an Ising-like interaction leaving the electron and Mn spins unchanged, and the second, flipping the Mn spin with simultaneous flipping of the electron spin to leave $M_Z + S_Z$ constant. The Ising-like terms of the electron-Mn interaction written in the basis of correlated exciton states take the form

$$\begin{aligned}\left\langle X^L_r \downarrow\Uparrow,M_Z\middle|\hat{H}_{e-\text{Mn}}\middle|X^{L'}_s \Uparrow\downarrow,M_Z\right\rangle &= \sum_{(ij)}^{N_L}\sum_{(kl)}^{N_{L'}} A^{*r}_{L;ij}A^s_{L';kl}\langle ij^L \downarrow\Uparrow,M_Z|\hat{H}_{e-\text{Mn}}|kl^{L'} \Uparrow\downarrow,M_Z\rangle \\ &= \sum_{(ij)}^{N_L}\sum_{(kl)}^{N_{L'}} A^{*r}_{L;ij}A^s_{L';kl}\frac{J^e_{i,l}(\vec{R})}{2}M_Z = \frac{1}{2}J^{e,\text{eff}}_{r,s}(\vec{R})M_Z, \qquad (5)\end{aligned}$$

where $J^{e,\text{eff}}_{r,s}(\vec{R}) = \sum_{(ij)}^{N_L}\sum_{(kl)}^{N_{L'}} A^{*r}_{L;ij}A^s_{L';kl}J^e_{i,l}(\vec{R})$ is the effective coupling constant constructed as a combination of single-particle exchange-coupling constants $J^e_{i,l}(\vec{R})$ weighted by their probability in the exciton wave function. All elements building the effective coupling constant, the wave function coefficients $A^r_{L;ij}$ and the single-orbital coupling constants $J^e_{i,l}(\vec{R})$, depend on the magnetic field. The matrix element of the electron-Mn Hamiltonian (4) reverses sign with reversed electron spin of an electron, e.g., $|X^{L'}_s \Uparrow\uparrow,M_Z\rangle$.

The spin-flipping matrix elements take the form

$$\begin{aligned}\left\langle X^L_r \downarrow\Uparrow,M_Z\middle|\hat{H}_{e-\text{Mn}}\middle|X^{L'}_s \Uparrow\uparrow,M'_Z\right\rangle &= \sum_{(ij)}^{N_L}\sum_{(kl)}^{N_{L'}} A^{*r}_{L;ij}A^s_{L';kl}\langle ij^L \downarrow\Uparrow,M_Z|\hat{H}_{e-\text{Mn}}|kl^{L'} \Uparrow\uparrow,M'_Z\rangle \\ &= -\sum_{(ij)}^{N_L}\sum_{(kl)}^{N_{L'}} A^{*r}_{L;ij}A^s_{L';kl}\frac{J^e_{i,l}(\vec{R})}{2}\langle M_Z|M^+|M'_Z\rangle \\ &= -\frac{1}{2}J^{e,\text{eff}}_{r,s}(\vec{R})\langle M_Z|M^+|M'_Z\rangle. \qquad (6)\end{aligned}$$

The Hamiltonian $\hat{H}_{h-\text{Mn}}$ (3) has only the Ising elements similar to diagonal elements for $\hat{H}_{e-\text{Mn}}$ and will be analyzed in detail later on.

We see that the magnetic-field dependence of the effective exchange constants $J^{e,\text{eff}}$ is due to the magnetic field dependence of exchange couplings $J^e_{i,l}(\vec{R})$ of orbitals $i,l$ and their occupation $A^{*r}_{L;ij}A^s_{L';kl}$ in the correlated exciton state. Both of these contributions change as the magnetic field is varied.

## IV. SPIN MODEL OF THE $X$-Mn COMPLEX

If we retain only the lowest single-particle level for the electron and the hole, then the correlated model of the $X$-Mn system (discussed in Sec. III) can be reduced to the simple spin model,[10,20,32] with the following Hamiltonian:

$$\begin{aligned}H = {} & g_{\text{Mn}}\mu_B\vec{B}\cdot\vec{M} + g_e\mu_B\vec{B}\cdot\vec{\sigma} + g_h\mu_B B_z j_z \\ & - J^e(R)\vec{\sigma}\cdot\vec{M} + J^h(R)j_z M_Z + H_{EHX}, \qquad (7)\end{aligned}$$

where $\vec{M}$, $\vec{\sigma}$, and $\vec{j}$ are the Mn, electron, and hole spin operators, respectively. The first three terms represent the Zeeman energies of the magnetic ion, the electron, and the hole, respectively, and $J^{e(h)} = J^{e(h)}_{00}(R)$ is the electron (hole) lowest single-particle state exchange coupling to the Mn ion at the position $R$, replaced by a phenomenological constant $J^{e(h)}$. The last term represents the electron-hole exchange, which in the basis of exciton states $(|+1\rangle,|-1\rangle,|+2\rangle,|-2\rangle)$ can be written as

$$H_{EHX} = \frac{1}{2}\begin{pmatrix} \Delta_0 & \Delta_1 & 0 & 0 \\ \Delta_1 & \Delta_0 & 0 & 0 \\ 0 & 0 & -\Delta_0 & \Delta_2 \\ 0 & 0 & \Delta_2 & -\Delta_0 \end{pmatrix}. \qquad (8)$$

The electron-hole interaction is parametrized by the bright-dark exciton splitting $\Delta_0$ and the anisotropic exchange splitting of the bright ($\Delta_1$) and dark ($\Delta_2$) exciton states. In the spin model all the exchange constants are parametrized at $B = 0$ and the dependence on the magnetic field enters only through the Zeeman terms.

## V. ABSORPTION AND EMISSION SPECTRA

Having obtained the eigenenergies and eigenfunctions of the electron-hole pair in the presence of the Mn ion, one can calculate the absorption and emission spectra from Fermi's golden rule:

$$I^{\pm}_{\varepsilon}(\omega) = \sum_f\sum_i P_i|\langle f|\hat{P}^{\pm}_{\varepsilon}|i\rangle|^2\delta(E_i - E_f \pm \omega), \qquad (9)$$

where $|i\rangle$ ($|f\rangle$) is the initial (final) state with corresponding energy $E_i$ ($E_f$), $P_i$ is the probability of initial state occupation: $P_i = \exp\{-\frac{E_i}{kT}\}/P_{\text{SUM}}$, with $P_{\text{SUM}} = \sum_i \exp\{-\frac{E_i}{kT}\}$, $k$ is the Boltzmann constant and $T$ temperature, while the interband

polarization operator $\hat{P}_{\varepsilon}^{\pm}$ annihilates $(-)$ or creates $(+)$ one electron-hole pair from the initial state with simultaneous emission $(-)$ or absorption $(+)$ of the photon with polarization $\varepsilon$. Depending on the spin $\sigma,\tau$ of removed particles, emitted photons have polarization $\varepsilon = \sigma_+$ ($\hat{P}^-_{\sigma+} = \sum_i c_{i\downarrow} h_{i\Uparrow}$), or $\varepsilon = \sigma_-$ ($\hat{P}^-_{\sigma-} = \sum_i c_{i\uparrow} h_{i\Downarrow}$) polarization.

In the calculations of emission and absorption spectra, Eq. (9), we assumed temperature much lower than the band gap of CdTe which assures that the conduction and valence band are empty of carriers in the absence of optical excitation. This implies that the initial states $|i\rangle$ in the emission spectra are the states of the interacting photoexcited exciton and a Mn ion (each of them being a linear combination of $|X^L_k,\tau\sigma,M_Z\rangle$ configurations), thermally populated with probability $P_i$. In the final state $|f\rangle$ we have an emitted photon and the Mn ion in any of its excited states $|M_Z\rangle$ with no carriers in the conduction and valence band due to the low temperature. Note that the interband polarization operator $P^-_{\varepsilon}$ annihilates an electron-hole pair in the initial state without changing the Mn $|M_Z\rangle$ state. Since the Mn state does not change, the Mn Zeeman energy does not contribute to the energy of the emitted photon.

On the other hand, in the calculations of the absorption spectra the initial states are the thermally populated states $|M_Z\rangle$ of the Mn ion in empty QD. The final states are all excited states of the exciton-Mn complex.

The main difference between absorption and emission occurs through the probability of occupation of the initial state $P_i$. In the absorption there are only six initial $|M_Z\rangle$ states thermally populated depending on the Mn Zeeman splitting, while there is a large number of final states for each $M_Z$ visible in the absorption spectra. On the other hand, in the emission process there are many $X$-Mn states; however, at low temperature only low-energy states are occupied, resulting in the visible emission only from the lowest excitonic shell.

## VI. RESULTS AND DISCUSSION

Here we illustrate the impact of correlations and the magnetic field on the absorption and emission spectra of a model quantum dot. Recent experiments and theory[34] indicate that in the CdTe quantum dots there are at least three confined electronic shells $s$, $p$, and $d$, and that the presence of these shells leads to qualitatively different effects, such as the quantum interference in the electronic structure of the $X$-Mn complex at $B = 0$. Hence all calculations were performed for CdTe quantum dots with $s$; $s,p$ and $s,p,d$ shells with the following parameters:[11,23,32,34] $\mathcal{R}^* = 12.11$ meV, $a_B = 5.61$ nm, and $\varepsilon = 10.6$, where the $s$-$p$ spacing is given by $\Omega_h + \Omega_e = 30$ meV, while $\Omega_e = 4\Omega_h$. The electron-Mn and hole-Mn bulk coupling constants are $J^h_{(0)} = 60$ meV nm$^3$ and $J^e_{(0)} = 15$ meV nm$^3$. The height of the QD is assumed to be $d = 2.56$ nm with manganese impurity in the center ($R = 0$). The Mn Landé factors are $g_e = -0.7$, $g_h = 0.38$, $g_{\mathrm{Mn}} = 2$, for the electron, the hole, and the Mn, respectively.

The electron-hole interaction is parametrized by the bright-dark exciton splitting $\Delta_0 = 0.5$ meV, the bright exciton splitting $\Delta_1 = 0.16$ meV, as well as the dark exciton splitting $\Delta_2 = 0$ meV. Figure 1 shows the results of calculated absorption spectra in the (a) correlated exciton-Mn model with $SPD$ shells, and (b) the spin model. The red dots (blue empty squares) correspond to the absorption of the $\sigma_-$ ($\sigma_+$) photons.

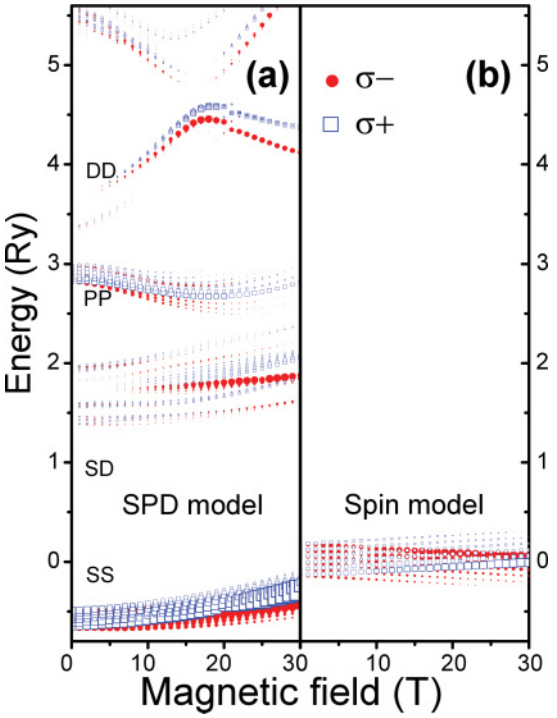


FIG. 1. (Color online) Magnetic field evolution of the absorption spectra calculated in a spin model (a) and correlated exciton model (b) which includes $s$, $p$, and $d$ single-particle shells and small anisotropy of the QD confining potential ($\gamma = 0.33$). In both QDs single-particle energies $\omega_e + \omega_h = 30$ meV; $\omega_e/\omega_h = 4$. Electron-hole exchange parameters as well as anisotropy parameters are chosen for SPD-correlated models to lead to bright exciton splitting $\Delta_1 = 0.16$ meV and bright-dark exciton splitting $\Delta_0 = 0.5$ meV. $\Delta_1$ and $\Delta_0$ are the parameters in the spin and $s$-shell models. Calculations are done for temperature of 75 K. The thickness of the lines represents the heights of the absorption peaks at a given energy.

The correlated exciton-Mn $SPD$ model is described in Sec. III. In the first step the excitonic Hamiltonian (1) is diagonalized in the basis of electron-hole configurations built out of the orbital states of three single-particle shells $s$, $p$, and $d$. Next, each exciton state is multiplied by all electron, hole, and Mn spin states. In the next step we limit our basis to correlated exciton states with energies below the energy cutoff $E_c$, which is varied to assure convergence of numerical results. In Fig. 1 we show the results of the diagonalization of the exciton-Mn Hamiltonian (2) with $E_c = 6.19\mathcal{R}^*$, the energy cutoff defined by the energy of the electron-hole configuration with both carriers on the $d$ shell and a total of $N_c = 768$ basis states. We note that due to the electron-hole exchange and the presence of Mn impurity all the correlated exciton-Mn basis states are coupled. As shown in Refs. 34 and 35, the essential configurations included in our basis involve electrons and holes on the $s$ shell (SS configurations), electrons (holes) on the $s$ shell and holes (electrons) on the $d$ shell (SD configurations), and electrons and holes on the $p$ shell (PP configurations).

From Fig. 1(a) we see that the absorption consists of three groups of lines corresponding to the absorption into the $s$

shell, $p$ shell, and $d$ shell. The $p$-shell absorption consists of lower-energy transitions involving SD configurations activated by the Coulomb interactions[34,35] and higher-energy PP states. The SD transitions correspond to zero angular momentum states and evolve in parallel with the emission from the $s$-shell states. The PP transitions are split by the Coulomb interactions and anisotropy, with the upper branch crossing the transitions associated with the $d$ shell. All excitonic transitions are "dressed" by the electron, hole, and Mn spin states. By contrast, the absorption in the spin model covers only the $s$ shell. The number of absorption lines in this energy range is equal to the number of absorption lines in the correlated exciton model; however, the spin model predicts only a linear magnetic field dependence through the Zeeman coupling. Hence, the correlated exciton model is necessary for the description of the higher-energy part of the absorption spectra. Coupling of $X$ with the Mn ion results in a characteristic absorption pattern allowing for the verification of the presence of the Mn ion in a quantum dot.

We now turn to the discussion of the emission spectra from the $s$ shell. Figure 2 compares the magnetic field evolution of the emission spectra calculated using different approximate models for the two circular polarizations. Panels show the calculated emission spectra in increasing degree of accuracy: (a) the spin model; (b) the $s$-shell model, with electron-hole configurations restricted to the $s$ shell but with

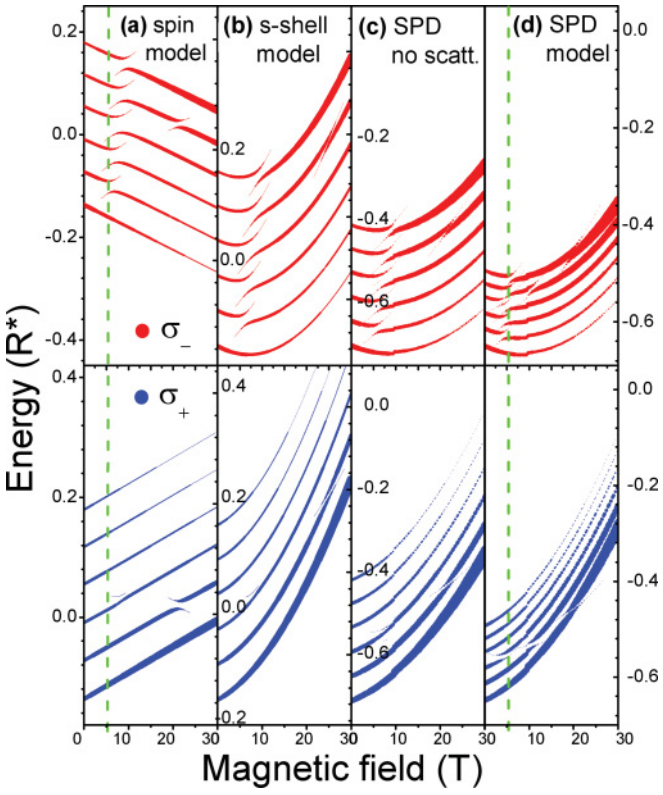


FIG. 2. (Color online) Magnetic field evolution of the emission spectra calculated using different models: (a) spin model, (b) $s$-shell model, (c) SPD-correlated exciton model, neglecting the scattering by Mn, and (d) full SPD-correlated exciton model. Parameters of all the QDs are the same as for Fig. 1. The thickness of the lines represents the heights of the absorption peaks at a given energy.

microscopic form of exciton-Mn interaction; (c) the SPD-correlated exciton model, with SS, SD, and DD configurations as described above, but with Mn not allowed to mix different electronic configurations [$i = j$ in the $H_{e\text{-Mn}}$ (4) and $H_{h\text{-Mn}}$ (3) part of the Hamiltonian]; and (d) the SPD-correlated exciton model including scattering by Mn as a spin-dependent impurity.

The emission spectra are different for the two polarizations and vary depending on different models used. Let us recall that there are $N_c = 24$ low-energy $X$-Mn configurations. In the spectra predicted by each model there are, however, six dominant emission lines for each polarization. At model-specific characteristic values of the magnetic field more features are visible due to anticrossings of emission lines.

In the spin model the only magnetic field dependence is linear through the Zeeman term. We note that current emission experiments combine the spin model spectra as shown here with an *ad hoc* diamagnetic term in order to fit the experimental spectra.[19,20] In the $s$-shell model the magnetic field dependence enters through the magnetic field dependence of the electron and hole $s$-shell energy levels, their Coulomb attraction, and through the magnetic field dependence of the $e$-Mn and $h$-Mn exchange-coupling constants $J^{e(h)}_{00,00}(R)$. The exchange coupling of the hole in the $s$ shell and for the Mn ion in the center[23] $J^{h}_{00,00}(0) = J^{h}_{2D}\frac{1}{2\pi}\frac{1}{l_h^{e2}}$ is inversely proportional to the area of the quantum dot, with explicit dependence on the magnetic field given by $J^{h}_{00,00}(0) = J^{h}_{2D}\frac{1}{2\pi}\sqrt{(\Omega^e_0)^2 + \frac{1}{4}(\Omega^e_c)^2}.J^{e(h)}_{00,00}$ increases with the magnetic field due to squeezing of the wave function toward the center of the QD. The rate of change with the magnetic field depends on the ratio of the hole cyclotron energy to the energy spacing of hole electronic shells.

Figure 2(c) shows the calculated excitonic emission spectrum with the correlated exciton state built out of the $s$, $p$, and $d$ shells. The interaction of the exciton with the Mn ion does not allow for the scattering by Mn as impurity. The final result is a slight decrease of the splitting of the emission lines in zero magnetic field due to a decreased occupation of the lowest-energy $s$-shell configuration in the exciton wave function and an increased population of $p$-shell orbitals which do not couple to Mn. This leads to a decrease of the $J^{h,\text{eff}}_{GS}$ and hence the effective magnetic field produced by the spin of the valence hole. However, inclusion of scattering by Mn, described previously in Ref. 34, leads to the QI effect. As calculated here, QI results in a significant decrease of the splitting of the emission lines as a function of the magnetic field, as shown in Fig. 2(d). Together with the decrease of the effective field produced by the hole, the electron-hole exchange becomes more visible in the emission spectra, since its strength becomes comparable to the exciton-Mn exchange coupling ($\Delta_1 = 0.16$ meV vs an average splitting of emission lines in the $SPD$ model of $\frac{1}{2}[J^e_{GS}(0) + 3J^h_{GS}(0)] = 0.38$ meV at zero magnetic field).

Details of the $\sigma_+$ emission spectra in the spin model and in the correlated exciton model for two selected values of $B$, $B = 0$, and $B = 5T$, are shown in Fig. 3. The magnetic field $B = 5T$ was chosen since for this magnetic field most of the anticrossings take place in the emission spectra shown in Fig. 2(d). The predicted line shape of the correlated exciton emission spectrum at $B = 0$ is similar to the spin model

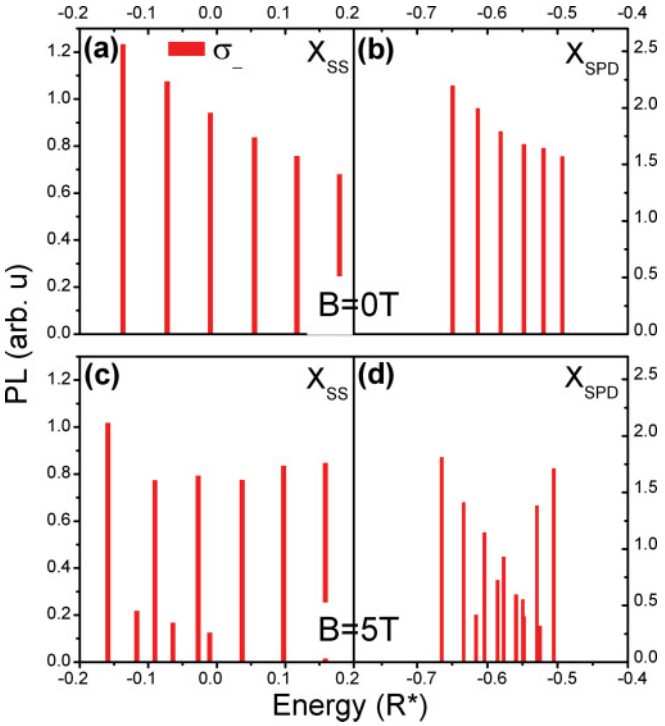


FIG. 3. (Color online) Comparison between calculated emission spectra in spin (left) and correlated exciton models (right) for zero magnetic field (upper panel) and magnetic field $B = 5$ T (lower panel) with the same parameters as for Fig. 1. Both models predict a splitting of the excitonic emission line into six $X$-Mn emission lines due to the interaction of the exciton with Mn; however, the quantitative splitting between lines is much different in these models. In the SPD model at $B = 5$ T there are more emission lines, since this is the magnetic field for which most of the anticrossings takes place in this model.

spectrum. The main difference is that the spacing of emission peaks is approximately half of the spacing in the spin model. However, the correlated exciton spectrum at $B = 5T$ is very different compared to the spin model. This is because the anticrossings of emission lines in the correlated model take place at a much smaller magnetic field, which is visible in Fig. 3, since the correlated exciton model leads to a smaller exchange coupling with Mn. The central crossing (subspace $M_Z + S_Z = 0$) takes place at $B = 5.25T$ for the SPD-correlated model instead of $B = 7.6T$ in the spin model. Hence the magnetic fields where crossings occur are a sensitive measure of the approximate model used.

Figure 4 identifies different emission peaks in the $\sigma_-$ polarization (upper panel) and compares the $\sigma_-$ emission spectrum with the calculated $\sigma_+$ emission spectrum (lower panel) for a magnetic field $B = 5T$. The $\sigma_-$ polarization spectrum has a very rich structure at this magnetic field. Peaks are labeled according to the final-state Mn spin projection. Since all of the anticrossings appear for that field, most of the peaks split into two. There are two exceptions: first peak with $M_Z = 5/2$ coming from the subspace with $M_Z + S_Z = 3$ which does not couple to any state through the spin-flip part of $H_{e\text{-Mn}}$ Hamiltonian, and the state with the final $M_Z = -1/2$ which appears three times in the $\sigma_-$ polarization spectrum. The reason for that is the electron-hole exchange mixing between this state, $|\Uparrow\downarrow, M_Z = -1/2\rangle$, in $\sigma_-$ polarization and state $|\Downarrow\uparrow, M_Z = -1/2\rangle$ in $\sigma_+$ polarization. This mixing is also visible on the lower panel of Fig. 4 since the emission line with $M_Z = -1/2$ is split into two lines having the same energy as the two lines in the $\sigma_-$ polarization spectrum. We see that the $\sigma_+$ emission spectrum is much simpler, due to the lack of the anticrossings between emission lines. This spectrum is also qualitatively similar to the emission spectra in the absence of the magnetic field for both polarizations with the only difference being the splitting of the $M_Z = -1/2$ emission line.

Let us now discuss the magnetic field evolution of the spacing of the peaks in the emission spectra shown in Fig. 2. We will discuss the average splitting of emission lines in $\sigma_+$ and $\sigma_-$ polarizations. The spin model assumes that the electron-Mn, hole-Mn, and electron-hole exchange constants do not change with the magnetic field. Since in the emission process the initial and final states correspond to the same $M_Z$ state of the Mn ion, the Zeeman energy cancels out and the spacing of the emission peaks shown in Fig. 5 in black does not change with the magnetic field. However, as discussed earlier the hole-Mn exchange coupling $J^h_{00,00}(0) = J^h_{2D}\frac{1}{2\pi}\sqrt{(\Omega^e_0)^2 + \frac{1}{4}(\Omega^e_c)^2}$ increases with the magnetic field. The splitting of the emission lines is directly proportional to the hole-Mn exchange coupling. Figure 5 shows the magnetic field dependence of the splitting of the emission lines based on the analytical expression for $J^h_{00,00}(0)(B)$ and on numerical calculation of the spacing of the emission peaks in the $s$-shell model (green dotted line and green empty dots, respectively).

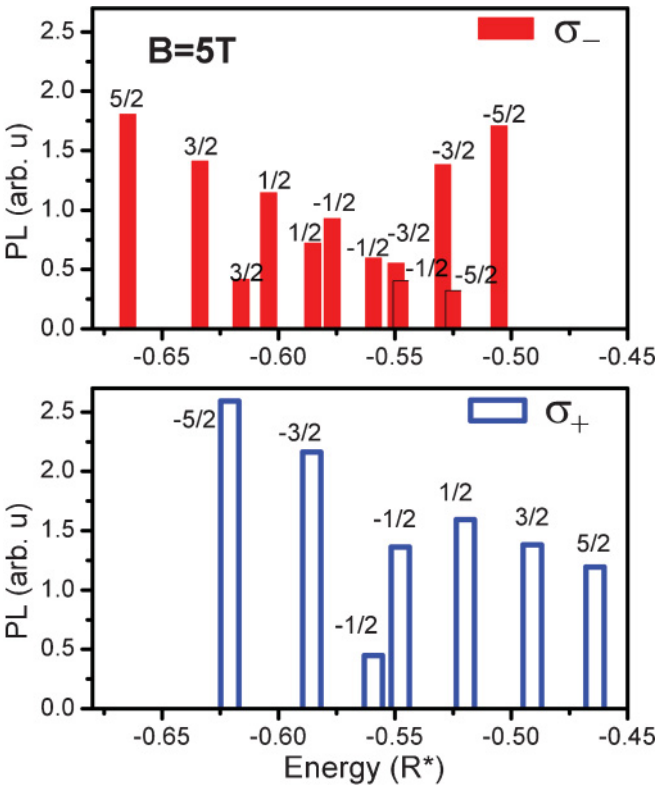


FIG. 4. (Color online) Comparison between calculated emission spectra in the correlated exciton model in $\sigma_-$ (upper panel) and $\sigma_+$ (lower panel) polarization for a small magnetic field $B = 5$ T with the same parameters as for Figs. 1 and 3.

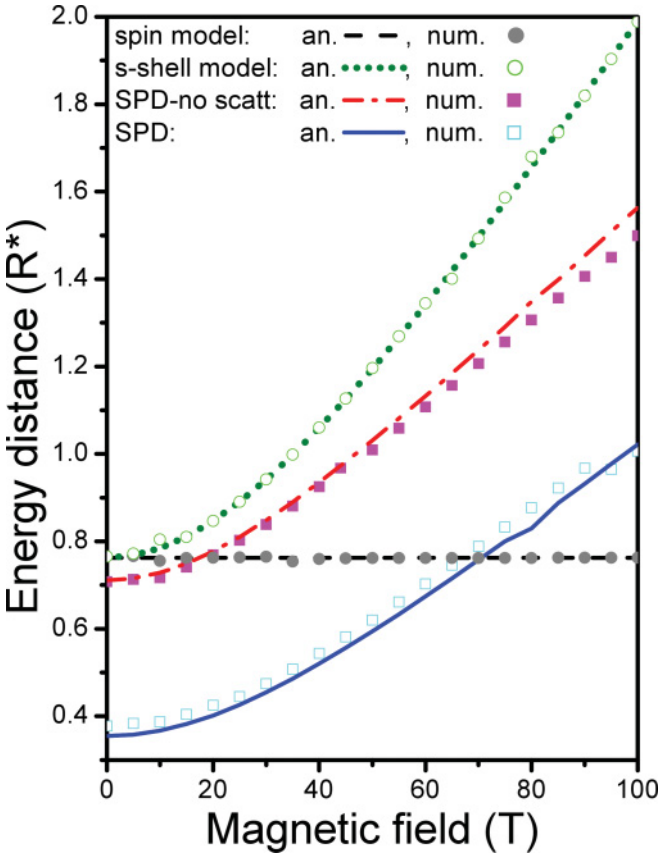


FIG. 5. (Color online) Magnetic field evolution of the average splitting of the emission lines calculated in different models: spin model, $s$-shell, and SPD model with and without Mn scattering. The in-between line spacing is calculated analytically as $\frac{1}{2}(J_{GS}^{e,\mathrm{eff}} + 3J_{GS}^{h,\mathrm{eff}})$ (solid, dashed, or dotted lines) based on the expectation values of $H_{h\text{-Mn}}$ and $H_{e\text{-Mn}}$ in the exciton's ground-state wave function (Ref. 34) and as an average splitting of emission lines from both $\sigma_+$ and $\sigma_-$ polarization calculated based on numerical emission spectra shown in Fig. 2 (symbols).

When we allow for the Coulomb scattering of the electron and hole to $s$, $p$, and $d$ shells the ground state of the exciton in a magnetic field becomes a linear combination of the electron-hole configurations[34]

$$|GS\rangle = A_{ss}(B)|SS\rangle + A_{pp}(B)|PP\rangle - A_{sd}(B)|SD\rangle + \cdots,$$

where $|SS\rangle$ is the lowest exciton configuration with both carriers on the $s$ shell, $|PP\rangle$ is the bright $p$-shell Jacobi coordinate[35] $|PP\rangle = 1/\sqrt{2}(|10,10\rangle + |01,01\rangle)$, and $|SD\rangle$ is the linear combination of the configurations with one carrier on the $s$ shell and the other on the state of the $d$ shell with angular momentum equal to zero: $|SD\rangle = 1/\sqrt{2}(|00,11\rangle + |11,00\rangle)$. The magnetic field $B$ changes both the energies of the HO states[38,39] as well as increases electron-hole Coulomb interactions. This changes the probabilities $A_{ss}(B), A_{pp}(B), A_{sd}(B)$ of occupation of the single-particle levels with increasing magnetic field and modifies the strength of exchange coupling of the electron and hole spin with the spin of the Mn ion. The Mn ion acts as an impurity and scatters carriers among single-particle states. With this scattering turned off, the resulting splitting of emission lines, calculated numerically, is shown in Fig. 5 as magenta squares. We see that in zero magnetic field there is a slight decrease of the emission line splitting due to the decreased population of the lowest exciton configuration and transfer of this probability to higher-energy configurations. The splitting increases with the magnetic field, but the correlations in the excitonic wave function lead to a decrease of the rate of increase of the peak splitting. For each magnetic field it is possible to calculate semianalytically the effective exciton-Mn interaction (emission line splitting) as $\frac{1}{2}(J_{GS}^{e,\mathrm{eff}} + 3J_{GS}^{h,\mathrm{eff}})$ using the exciton ground-state wave function in Eq. (5). In Fig. 5 we show these calculations with the red dot-dashed line which shows only a slight deviation from the full numerical calculations. This deviation is due to the fact that the semianalytical solution does not include the anisotropy of the QD, electron-hole exchange, or interaction with higher exciton states. However, it is instructive to see that this simplified calculation gives qualitatively the same result as a complicated numerical calculation.

The splitting of emission lines calculated in the $SPD$ model accounting for the scattering by the Mn ion is shown as the blue solid line and light-blue empty squares (analytical and numerical calculations, respectively) in Fig. 5. The quantum interference effect causes a significant decrease of the splitting of the emission lines[34] due to the reduction of the effective magnetic field produced by the hole, leading to the "exchange" splitting of different $M_Z$ states: $\langle H_{h\text{-Mn}}\rangle = \langle M_Z|\langle\downarrow\Uparrow|\langle GS|H_{h\text{-Mn}}|GS\rangle|\Uparrow\downarrow\rangle|M_Z\rangle$. To reduce the hole exchange field both the electron-hole Coulomb interaction, leading to the presence of SD configuration in the excitonic ground state, as well as the scattering by the Mn impurity have to be present simultaneously.

Comparison between the green, dotted and blue, solid lines shows that not only the magnitude of the splitting decreases, but that correlations lead to the decrease of the rate of growth of the splitting with increasing magnetic field. Current experiments probe the emission spectrum of CdTe quantum dots in magnetic fields up to 30 T. As can be seen from Fig. 5, the magnetic field dependence of the splitting of the emission peaks is weak in this magnetic field range. Much higher magnetic fields, of the order of 100 T, are required to distinguish the different theoretical treatments of the emission spectrum.

## VII. SUMMARY

In summary, we presented a microscopic theory which can be used to describe the magnetic field dependence of the optical properties of semimagnetic semiconductor quantum dots containing a single magnetic impurity, Mn, as a function of quantum dot shell structure, anisotropy, and impurity position. All direct, short-, and long-range exchange electron-hole Coulomb interactions as well as the electron and hole exchange interaction with the magnetic impurity were included. The absorption and emission spectrum is predicted as a function of the photon energy, magnetic field, quantum dot shell structure, and anisotropy. The results of calculated absorption and emission spectra as a function of the magnetic field up to

100 T were presented for slightly elliptical quantum dots with a single Mn ion in the center. It was shown that the electron-hole correlations and scattering by the Mn ion play a significant role in determining optical properties. In particular, it was shown that while the magnetic field enhances the interaction of exciton with the Mn ion leading to a magnetic-field-induced increase in the spacing of emission peaks, the magnetic-field-induced increase of Coulomb interactions and correlations in the $X$-Mn system cancels the increase in the $X$-Mn coupling. This cancellation makes the spin model superficially agree with experiment. To distinguish between phenomenological spin and correlated exciton models, either absorption spectra or emission spectra in higher magnetic fields are needed.

Future work should include the effects of light hole-heavy hole mixing, a higher number of excitons and Mn ions, Mn position, and, ultimately, fully microscopic, atomistic models[53] of semimagnetic quantum dots.

## ACKNOWLEDGMENTS

The authors thank NSERC, NRC-CNRS CRP, Canadian Institute for Advanced Research, and QuantumWorks for support.

[1] A. J. Heinrich, J. A. Gupta, C. P. Lutz, and D. M. Eigler, Science **306**, 466 (2004).
[2] M. Ciorga, A. S. Sachrajda, P. Hawrylak, C. Gould, P. Zawadzki, S. Jullian, Y. Feng, and Z. Wasilewski, Phys. Rev. B **61**, R16315 (2000).
[3] K. Ono, D. G. Austing, Y. Tokura, and S. Tarucha, Science **297**, 1313 (2002).
[4] J. M. Elzerman, R. Hanson, L. H. Willems van Beveren, B. Witkamp, L. M. K. Vandersypen, and L. P. Kouwenhoven, Nature (London) **430**, 431 (2004).
[5] J. Petta, A. Johnson, J. Taylor, E. Laird, A. Yacoby, M. D. Lukin, C. M. Marcus, and M. P. Hanson, Science **309**, 2180 (2005).
[6] A. Kudelski, A. Lemaitre, A. Miard, P. Voisin, T. C. M. Graham, R. J. Warburton, and O. Krebs, Phys. Rev. Lett. **99**, 247209 (2007).
[7] D. Kitchen, A. Richardella, J.-M. Tang, M. E. Flatte, and A. Yazdani, Nature (London) **442**, 436 (2006).
[8] D. A. Bussian, S. A. Crooker, M. Yin, M. Brynda, A. L. Efros, and V. I. Klimov, Nature Mater. **8**, 35 (2008).
[9] S. T. Ochsenbein and D. R. Gamelin, Nat. Nanotechnol. **6**, 112 (2011).
[10] L. Besombes, Y. Leger, L. Maingault, D. Ferrand, H. Mariette, and J. Cibert, Phys. Rev. Lett. **93**, 207403 (2004).
[11] J. K. Furdyna, J. Appl. Phys. **64**, R29 (1988).
[12] *Introduction to the Physics of Diluted Magnetic Semiconductors*, edited by J. Kossut and J. A. Gaj (Springer, New York, 2010).
[13] P. Hawrylak, M. Grabowski, and J. J. Quinn, Phys. Rev. B **44**, 13082 (1991).
[14] L. Besombes, Y. Leger, J. Bernos, H. Boukari, H. Mariette, J. P. Poizat, T. Clement, J. Fernández-Rossier, and R. Aguado, Phys. Rev. B **78**, 125324 (2008).
[15] C. Le Gall, R. S. Kolodka, C. L. Cao, H. Boukari, H. Mariette, J. Fernandez-Rossier, and L. Besombes, Phys. Rev. B **81**, 245315 (2010).
[16] M. Goryca, T. Kazimierczuk, M. Nawrocki, A. Golnik, J. A. Gaj, P. Kossacki, P. Wojnar, and G. Karczewski, Phys. Rev. Lett. **103**, 087401 (2009).
[17] A. Hundt, J. Puls, and F. Henneberger, Phys. Rev. B **69**, 121309(R) (2004).
[18] J. Fernández-Rossier, Phys. Rev. B **73**, 045301 (2006).
[19] Y. Leger, L. Besombes, L. Maingault, D. Ferrand, and H. Mariette, Phys. Rev. Lett. **95**, 047403 (2005).
[20] M. Goryca, P. Plochocka, T. Kazimierczuk, P. Wojnar, G. Karczewski, J. A. Gaj, M. Potemski, and P. Kossacki, Phys. Rev. B **82**, 165323 (2010).
[21] A. L. Efros, M. Rosen, and E. I. Rashba, Phys. Rev. Lett. **87**, 206601 (2001).
[22] J. Fernández-Rossier and R. Aguado, Phys. Rev. Lett. **98**, 106805 (2007).
[23] F. Qu and P. Hawrylak, Phys. Rev. Lett. **95**, 217206 (2005).
[24] F. Qu and P. Hawrylak, Phys. Rev. Lett. **96**, 157201 (2006).
[25] J. Fernández-Rossier and L. Brey, Phys. Rev. Lett. **93**, 117201 (2004).
[26] A. O. Govorov, Phys. Rev. B **72**, 075359 (2005).
[27] R. M. Abolfath, P. Hawrylak, and I. Zutic, Phys. Rev. Lett. **98**, 207203 (2007).
[28] N. T. T. Nguyen and F. M. Peeters, Phys. Rev. B **78**, 045321 (2008).
[29] N. T. T. Nguyen and F. M. Peeters, Phys. Rev. B **78**, 245311 (2008).
[30] N. T. T. Nguyen and F. M. Peeters, Phys. Rev. B **83**, 075419 (2011).
[31] A. O. Govorov and A. V. Kalameitsev, Phys. Rev. B **71**, 035338 (2005).
[32] S.-J. Cheng and P. Hawrylak, Europhys. Lett. **81**, 37005 (2008).
[33] D. E. Reiter, T. Kuhn, and V. M. Axt, Phys. Rev. Lett. **102**, 177403 (2009).
[34] A. H. Trojnar, M. Korkusinski, E. S. Kadantsev, P. Hawrylak, M. Goryca, T. Kazimierczuk, P. Kossacki, P. Wojnar, and M. Potemski, Phys. Rev. Lett. **107**, 207403 (2011).
[35] P. Hawrylak, G. A. Narvaez, M. Bayer, and A. Forchel, Phys. Rev. Lett. **85**, 389 (2000).
[36] M. Bayer, O. Stern, P. Hawrylak, S. Fafard, and A. Forchel, Nature (London) **405**, 923 (2000).
[37] A. H. Trojnar, E. S. Kadantsev, M. Korkusinski, and P. Hawrylak, Phys. Rev. B **84**, 245314 (2011).
[38] S. Raymond, S. Studenikin, A. Sachrajda, Z. Wasilewski, S. J. Cheng, W. Sheng, P. Hawrylak, A. Babinski, M. Potemski, G. Ortner, and M. Bayer, Phys. Rev. Lett. **92**, 187402 (2004).
[39] S.-J. Cheng, W. Sheng, and P. Hawrylak, Phys. Rev. B **68**, 235330 (2003).
[40] A. Wojs, P. Hawrylak, S. Fafard, and L. Jacak, Phys. Rev. B **54**, 5604 (1996).
[41] P. Hawrylak, Phys. Rev. Lett. **71**, 3347 (1993).
[42] A. Wojs and P. Hawrylak, Phys. Rev. B **53**, 10841 (1996).
[43] M. Bayer, G. Ortner, O. Stern, A. Kuther, A. A. Gorbunov, A. Forchel, P. Hawrylak, S. Fafard, K. Hinzer, T. L. Reinecke,

S. N. Walck, J. P. Reithmaier, F. Klopf, and F. Schafer, Phys. Rev. B **65**, 195315 (2002).
[44]D. Chithrani, M. Korkusinski, S.-J. Cheng, P. Hawrylak, R. L. Williams, J. Lefebvre, P. J. Poole, and G. C. Aers, Physica E **26**, 322 (2005).
[45]E. S. Kadantsev, M. Zielinski, M. Korkusinski, and P. Hawrylak, J. Appl. Phys. **107**, 104315 (2010).
[46]P. Hawrylak, Solid State Commun. **88**, 475 (1993).
[47]A. Wojs and P. Hawrylak, Phys. Rev. B **51**, 10880 (1995).
[48]T. Takagahara, Phys. Rev. B **47**, 4569 (1993).
[49]T. Takagahara, Phys. Rev. B **62**, 16840 (2000).
[50]S. V. Goupalov and E. L. Ivchenko, Phys. Solid State **43**, 1867 (2001).
[51]E. S. Kadantsev and P. Hawrylak, Phys. Rev. B **81**, 045311 (2010).
[52]E. S. Kadantsev and P. Hawrylak, J. Phys.: Conf. Ser. **248**, 012018 (2010).
[53]M. Zielinski, M. Korkusinski, and P. Hawrylak, Phys. Rev. B **81**, 085301 (2010).